Measurement of correlation-enhanced collision rates using pure ion plasmas[a)]

F. Anderegg, C. F. Driscoll,[b)] D. H. E. Dubin, and T. M. O'Neil
Department of Physics, University of California at San Diego, 9500 Gilman Drive, La Jolla, California 92093, USA

(Received 19 November 2009; accepted 23 December 2009; published online 26 January 2010)

This paper presents the first direct experimental measurements of the Salpeter enhancement of collisions due to particle correlations. The perpendicular-to-parallel collision rate $\nu_{\perp\|}$ is measured in laser-cooled pure ion plasmas, spanning the regimes from weak to strong magnetization, and from weak to strong particle correlations. The abrupt suppression of collisions in the strongly magnetized regime of $T \lesssim 10^{-3}$ eV is observed, mitigated by the Salpeter enhancement when correlation effects become significant. This $\nu_{\perp\|}$ enhancement due to correlations is directly analogous to the enhancement of fusion collisions in hot dense stellar plasmas. The measured collisional enhancement is approximately $\exp(\Gamma)$, where Γ is the correlation parameter, and this is quantitatively consistent with analytical estimates based on thermal equilibrium shielding and correlations. © *2010 American Institute of Physics*. [doi:10.1063/1.3293131]

I. INTRODUCTION

This paper presents the first direct experimental measurements of the Salpeter collisional enhancement factor in a strongly correlated plasma. This factor is predicted to enhance nuclear reaction rates in hot dense strongly correlated plasmas, such as those found in giant planet interiors, brown dwarfs, and degenerate stars;[1–10] and recent theory[11] establishes that it also applies to the perpendicular-to-parallel collisions in cryogenic magnetized plasmas considered here.[12]

Direct laboratory observation of nuclear reaction rates in strongly correlated plasmas would require prohibitively high temperatures (for measurable rates) and densities (for correlation effects). Instead, we measure the analogous Salpeter enhancement of perp-to-parallel energy equipartition in a strongly magnetized, *cryogenic*, pure ion plasma. The collisional equipartition rate $\nu_{\perp\|}$ will be seen to involve a dynamical factor $I(\bar{\kappa})$ representing magnetization effects, and an equilibrium screening enhancement factor $f(\Gamma)$ representing correlation effects.

Strong magnetization means that the thermal cyclotron radius $r_c \equiv \bar{v}/\Omega_c$ is small compared to the mean distance of closest approach $b \equiv e^2/T$. (Here, $\bar{v} \equiv \sqrt{T/m}$ and $\Omega_c = eB/mc$.) In this regime, the kinetic energy $E_\perp$ of cyclotron motion of colliding pairs is an adiabatic invariant, and perp-to-parallel collisions are strongly suppressed; the dynamical factor $I(\bar{\kappa})$ becomes exponentially small when $\bar{\kappa} \equiv \sqrt{2}b/r_c \gg 1$. In these strongly magnetized plasmas, $E_\perp$ is exchanged with parallel energy $E_\|$ only through rare close binary collisions that break the $E_\perp$ adiabatic invariant,[13–15] in direct analogy with nuclear energy liberated through close collisions.[11]

The correlation enhancement is caused by plasma screening of the repulsive Coulomb potential between charges, allowing closer collisions for a given relative energy. The enhancement factor $f(\Gamma)$ is predicted to be large when the plasma correlation parameter $\Gamma \equiv e^2/aT$ is larger than unity, scaling as $f(\Gamma) \sim e^{\Gamma}$. Here a is the Wigner–Seitz radius defined in terms of density n as $(4/3)\pi n a^3 = 1$. The equipartition rate $\nu_{\perp\|}$ is seen to be enhanced by plasma screening in exactly the same way as the nuclear reaction rate in two regimes: the weakly correlated regime $\Gamma \ll 1$ and the strong-screening regime $1 \lesssim \Gamma \ll \bar{\kappa}^{+2/5}$. The analogy does not extend to the "pycnonuclear" regime where collective effects determine the collisionality.

This analogy is surprising because the rates are controlled by very different processes (nuclear reactions versus breaking of an adiabatic invariant) in very different plasmas, for which the densities and temperatures differ by many orders of magnitude. Nevertheless, $f(\Gamma)$ is the same for both rates because the rates are dominated by close collisions, and the enhancement measures the increase in probability of such close collisions due to plasma screening. Furthermore, $f(\Gamma)$ is a thermal equilibrium quantity predicted for a classical plasma to depend on temperature and density only through the single parameter Γ; so fusing ions in an astrophysical fusion plasma can be modeled by a cryogenic plasma with the same Γ value. The present experiments corroborate that $f(\Gamma)$ is independent of the dynamical magnetization parameter $\bar{\kappa}$.

The $I(\bar{\kappa})$ suppression of perp-to-parallel collisionality in strongly magnetized plasmas has been extensively analyzed theoretically and has been observed in prior experiments with cryogenic pure electron plasmas. However, correlation effects were negligible in these electron plasmas. In contrast, pure ion plasmas are routinely laser cooled into the correlated liquid and crystalline regime. Jensen *et al.*[16] reported enhanced collisionality with impurity ions in a beryllium ion plasma with $\Gamma = 170$, and the inferred collisionality was roughly ten orders of magnitude greater than predicted by models neglecting correlations. However, these experiments

[a)]Paper UI3 1, Bull. Am. Phys. Soc. **54**, 300 (2009).
[b)]Invited speaker.

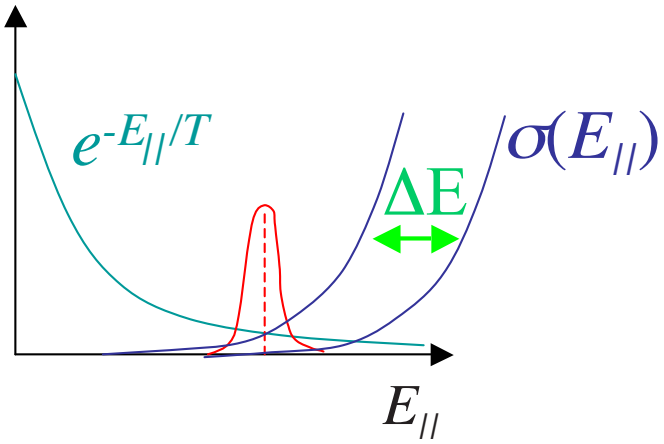

FIG. 1. (Color online) The product of an exponentially decaying Maxwellian and an exponentially growing cross-section σ gives the Gamow peak. Shifting σ by ΔE gives enhancement $\exp(\Delta E/T)$.

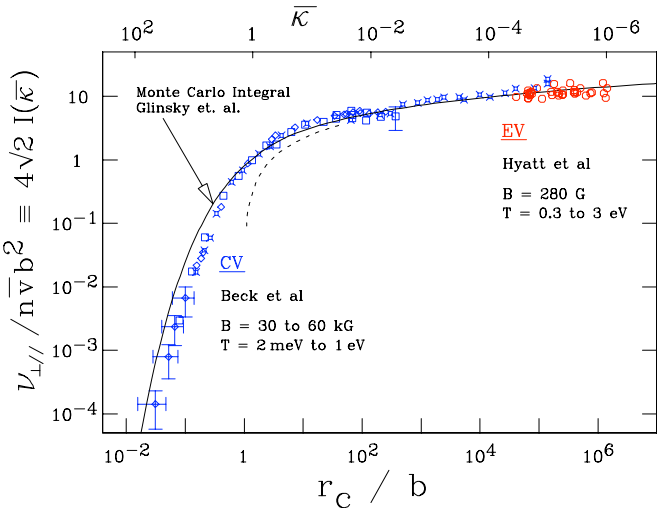

FIG. 2. (Color online) Magnetization factor $I(\bar{\kappa})$ vs $r_c/b=\sqrt{2}/\bar{\kappa}$. Monte Carlo integral analysis (solid curve) corrects $\ln(r_c/b)$ approximation (dashed curve) for $r_c \lesssim b$. Data from high-B cryogenic electrons (CV) and low-B warm electrons (EV) show close correspondence to theory.

were in the classical pycnonuclear regime of $\Gamma > \bar{\kappa}^{+2/5}$, where no theory of $f(\Gamma)$ has been developed.

II. THEORY

We consider first the dynamical effects of magnetization expressed as $I(\bar{\kappa})$, then the equilibrium effects of correlation expressed as $f(\Gamma)$, writing

$$\nu_{\perp\|} = n\bar{v}b^2 4\sqrt{2} I(\bar{\kappa}) f(\Gamma). \tag{1}$$

The high temperature range of $T > 10^{-3}$ eV represents the "normal," weakly magnetized regime of $r_c \gg b$ (or $\bar{\kappa} \ll 1$), where the perp-to-parallel collision rate is $\nu_{\perp\|} = (8/15)\sqrt{\pi} n\bar{v}b^2 \ln\Lambda$. Here, $\ln\Lambda$ represents the integrated collisional dynamics over impact parameters $b < \rho < r_c$; it is most accurately given by[14] $\ln\Lambda = \ln(r_c/b) + 0.75$, as described below. In this regime, perp-to-parallel energy sharing takes place via collisions at all energies in the Maxwellian distribution.

At lower temperatures (here $T \sim 10^{-3}$ eV), the cyclotron radius r_c becomes comparable to the distance of closest approach b, and the perp-to-parallel collision rate decreases. For $T \lesssim 10^{-3}$ eV, the parallel dynamics become much slower than the cyclotron dynamics, the two-particle perpendicular energy $E_\perp = E_{\perp 1} + E_{\perp 2}$ is an adiabatic invariant, and only rare, energetic collisions cause energy sharing between $E_\perp$ and $E_\|$.

In this strongly magnetized regime, the equipartition rate $\nu_{\perp\|}$ is the integral over a product of the Maxwellian distribution describing the relative energy of colliding pairs, and a collisional cross-section $\sigma(E_\|)$ describing the change in the cyclotron adiabatic invariant for collisions with relative energy $E_\|$. This is illustrated schematically in Fig. 1. The cross-section σ increases exponentially with $E_\|$, as

$$\sigma(E_\|) \propto e^{-\pi\Omega_c b_{\|}/v_{\|}} = e^{-(E_\Omega/E_\|)^{3/2}}, \tag{2}$$

with the characteristic energy

$$E_\Omega/T = (\pi\sqrt{2} b/r_c)^{2/3} \equiv (\pi\bar{\kappa})^{2/3}. \tag{3}$$

The overall collision rate is then given by

$$\nu_{\perp\|}(T) = \int dE_\| \frac{1}{T} e^{-E_\|/T} \sigma(E_\|). \tag{4}$$

The product of the exponentially increasing σ with the exponentially decreasing Maxwellian leads to a Gamow peak in the differential collision rate, at a Gamow energy

$$E_G = 1.23\bar{\kappa}^{2/5} T. \tag{5}$$

This collisional dynamics was analyzed and simulated by Glinsky in 1992.[14] For $\bar{\kappa} \ll 1$, the traditional plasma collisionality is

$$I(\bar{\kappa}) \to (\sqrt{2\pi}/15)[\ln(\sqrt{2}/\bar{\kappa}) + 0.75], \tag{6}$$

and for $\bar{\kappa} > 1$ one obtains exponential suppression, which can be expressed as

$$I(\bar{\kappa}) \equiv i(\bar{\kappa}) \exp(-2.044\bar{\kappa}^{2/5}). \tag{7}$$

Here,

$$i(\bar{\kappa}) = \{1.83\bar{\kappa}^{-7/5} + 20.9\bar{\kappa}^{-11/15} + 0.347\bar{\kappa}^{-13/15} + 87.8\bar{\kappa}^{-1} + 6.68\bar{\kappa}^{-17/5} + \cdots\} \tag{8}$$

for $\bar{\kappa} > 10^2$, and

$$i(\bar{\kappa}) \sim 1.5 \quad \text{for} \quad \bar{\kappa} < 10. \tag{9}$$

In comparing theory to experiment, we use formulas (6)–(8) in their respective regimes of validity and for intermediate $\bar{\kappa}$ values we use a numerical fit to the equipartition data of Glinsky *et al.*,[14] found in Table I of their paper. Figure 2 shows the Glinsky calculation as a solid curve and shows the simple $\ln(r_c/b)$ approximation as a dashed curve for comparison. The prior measurements[17] of $\nu_{\perp\|}$ from two separate pure electron plasma apparatuses operating in disparate plasma regimes show close overall correspondence with the theory. The slight disagreement at low temperatures could represent a factor of 1.6 systematic error in measuring tem-

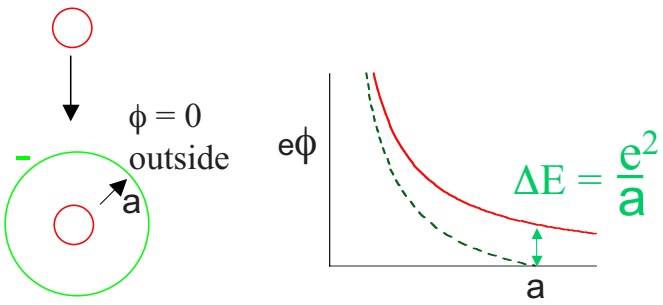

FIG. 3. (Color online) Collisional energy shift ΔE from two species (atomic) shielding. Single species ion plasmas have ΔE from a correlation deficit of ions.

perature, or could represent underpopulation of the electron distributions at energies $E_G \gtrsim 3$ T.

Interparticle correlations have the effect of enhancing these rare, energetic collisions, by reducing the relative kinetic energy $E_\parallel$ required for a close collision with given distance of closest approach. Reducing the requisite $E_\parallel$ by an amount ΔE shifts the $\sigma(E_\parallel)$ curve of Fig. 1, increasing the product with the Maxwellian by a factor $f \sim e^{\Delta E/T}$. This enhancement takes various forms depending on the nature of the correlation or shielding effects.

Figure 3 illustrates a conceptually simple type of shielding, that of atomic electrons shielding a nucleus. Without the electrons, two colliding nuclei of charge $+e$ separated by a distance ρ would experience a potential energy barrier $e\phi(\rho)=e^2/\rho$. A thin shell of shielding charge $-e$ at $r=a_0$ makes $\phi(\rho)=0$ for $\rho>a_0$, reducing the potential energy barrier by $\Delta E=e^2/a_0$. That is, a given close impact with $\rho<a$ requires ΔE less initial relative kinetic energy $E_\parallel$, and the probability of close collisions is enhanced. Note that the energy shift ΔE arises from shielding at large distances, even though the impact parameter is small.

For the single-species pure ion plasmas considered here, the correlation effects are a continuum between weak Debye shielding over distances $\lambda_D \equiv (T/4\pi ne^2)^{1/2}$ at high temperatures, and lattice potentials over interparticle spacing distances $a \equiv (3/4\pi n)^{1/3}$ at low temperatures. In the weakly correlated Debye shielding limit, the energy required for a close collision at distance of closest approach $\rho<b<\lambda_D$ is

$$E = \left(\frac{e^2}{\rho}\right) e^{-\rho/\lambda_D} \approx \frac{e^2}{\rho} - \frac{e^2}{\lambda_D}, \tag{10}$$

and the collisional enhancement arises from $\Delta E=e^2/\lambda_D$, as

$$f \sim \exp(e^2/\lambda_D T). \tag{11}$$

Of course, in these single species ion plasmas, the Debye shielding "cloud" is a region of lesser ion density rather than a cloud of oppositely charged electrons. As the temperature decreases, λ_D decreases and b increases, with ratio $b/\lambda_D = \sqrt{3}T^{3/2}$.

In the strong coupling regime of $\Gamma>1$, the effective shielding distance is the interparticle spacing, and the energy required for a collision at distance $\rho<a$ is

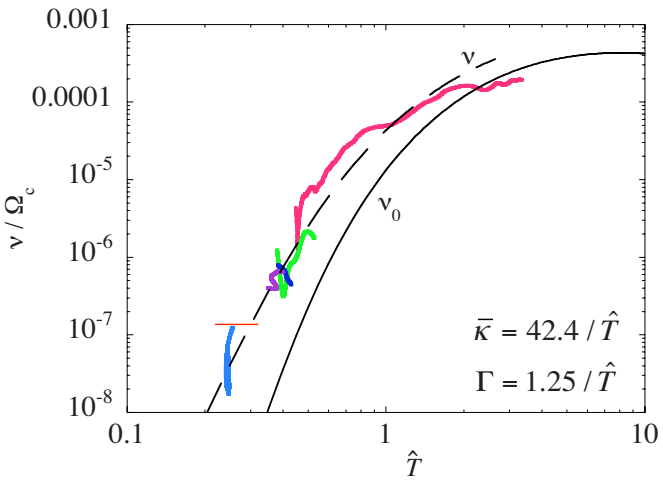

FIG. 4. (Color online) Equipartition rate vs scaled temperature for several simulations, compared to theory with (dashed curve) and without (solid curve) screening. The enhancement factor is modeled by Eq. (15).

$$E_\parallel = e^2/\rho - e^2/a. \tag{12}$$

This gives collisional enhancement

$$f(\Gamma) \sim e^{e^2/aT} = e^\Gamma, \tag{13}$$

again arising from ΔE due to shielding at large distances. A more rigorous derivation of the enhancement factor using a Green–Kubo expression[11] for the equipartition rate provides an expression for f in terms of partition functions,

$$f(\Gamma) = VZ_{U_{N-1}}(n)/Z_{U_N}(0), \tag{14}$$

where V is the volume, and $Z_{U_N}(n)$ is the configurational portion of the canonical partition function for a system of N charges, n of which have charge $2e$. This expression is identical to one derived previously for nuclear reactions in the strong and weak-screening regimes.[8] For $\Gamma \ll 1$ it matches the weak-screening result, Eq. (11). For $\Gamma>1$ the expression has been evaluated by different authors using Monte Carlo methods.[6,7,9,10] Three such expressions, valid for $\Gamma \gtrsim 1$, are

$$\ln f(\Gamma) = 1.148\ \Gamma - 0.009\,44 \ln \Gamma - 0.000\,168\ \Gamma^2 \quad \text{(Ichimaru)}, \tag{15}$$

$$\ln f(\Gamma) = 1.132\ \Gamma - 0.0094\ \Gamma \ln \Gamma \quad \text{(Ogata)}, \tag{16}$$

and

$$\ln f(\Gamma) = 1.056\,299\ \Gamma + 1.039\,957\ \Gamma^{0.323\,064} - 0.545\,823 \ln \Gamma - 1.1323 \quad \text{(DeWitt)}. \tag{17}$$

At large Γ, $\ln f$ is roughly linear in Γ, as expected from the estimate of Eq. (13).

Prior molecular-dynamics simulations[11] of perp-parallel equipartition in spheroidal clouds of 200–500 charges were consistent with the predicted enhancement factor. Figure 4 shows the equipartition rates $\nu_{\perp\parallel}$ obtained from various simulation scenarios, compared to the unshielded rate ν_0 (solid curve) and the shielding-enhanced rate ν (dashed curve). The dimensionless temperature $\hat{T}$ in the simulations is scaled to simulation parameters, and is related to $\bar{\kappa}$ and Γ

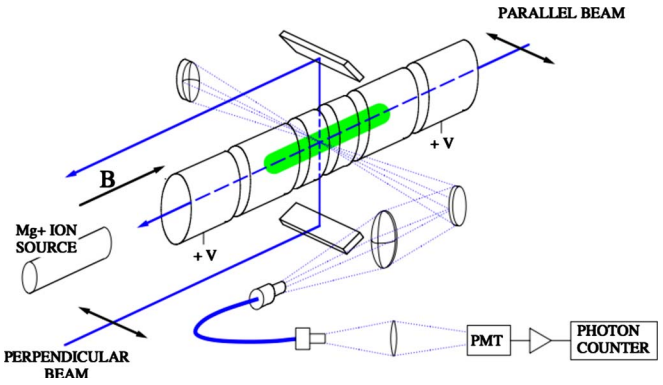

FIG. 5. (Color online) Schematic of the cylindrical IV apparatus and Mg^+ pure ion plasma, showing perpendicular and parallel laser diagnostic and cooling.

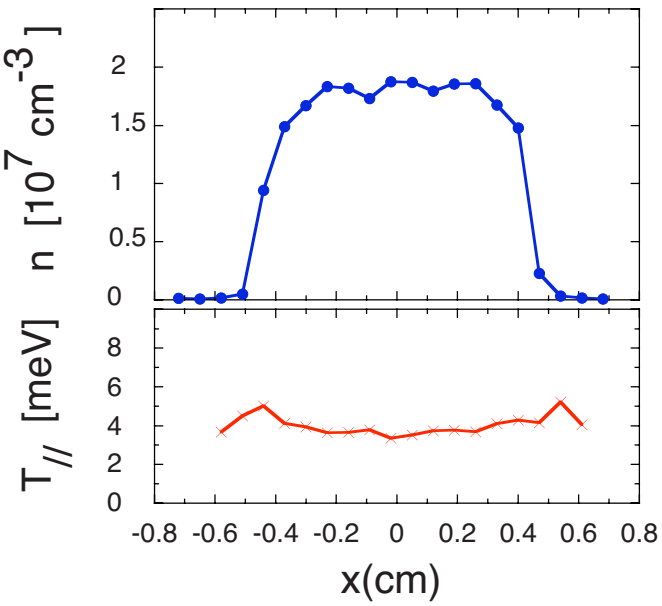

FIG. 6. (Color online) Typical density profile $n(r)$ and temperature profile $T(r)$ for higher density plasmas in the meV temperature range.

as shown in the figure. These results provided strong support for theory well into the strong shielding regime, despite issues regarding the small number of particles at energies $E \gtrsim 10$ T, where the Gamow peak is situated.

III. ION PLASMA EXPERIMENTS

Here we obtain quantitative collision rates versus temperature and density utilizing pure magnesium ion plasmas in a cylindrical Penning–Malmberg trap, as shown in Fig. 5. The plasmas consist of $N_{\mathrm{tot}} \sim 10^8$ Mg^+ ions in a column length $L_p \sim 10$ cm and radius $R_p \sim 0.4-1.1$ cm, inside cylindrical electrodes with wall radius $R_w = 2.86$ cm. A uniform axial magnetic field of 1.2 or 3.0 Tesla provides radial confinement of the ions, and positive voltages $V_c \sim 200$ V applied to end electrodes provide axial confinement.

The plasma density n and temperatures $T_\parallel$ and $T_\perp$ are diagnosed with laser induced fluorescence techniques. The fluorescence signal versus laser frequency is fit to a "Voigt" profile[18] encompassing the Lorentzian linewidth of the transition and the Maxwellian distribution due to Doppler broadening from thermal motion. Figure 6 shows typical profiles of density $n(r)$ and parallel temperature $T_\parallel(r)$, with $n_0 \sim 1.8 \times 10^7$ and $T_\parallel \sim 4$ meV; lower density plasmas with $n_0 \sim 0.12 \times 10^7$ would have $R_p \sim 1.1$ cm.

The ion plasmas relax toward thermal equilibrium in the $\mathbf{E} \times \mathbf{B}$ drift rotating frame, with $f_E \sim 5$ kHz $(n/10^7\ \mathrm{cm}^{-3})$. Static θ-asymmetries in the trapping magnetic and/or electric fields cause a weak "drag" on the plasma, as do ion-neutral momentum-transfer collisions at rate $\nu_{iN} \sim 2.5 \times 10^{-3}$/s from base pressure $P_N \sim 10^{-10}$ Torr. A weak "rotating wall" voltage[19,20] applied to θ-sectored electrodes is used to provide a positive torque, which counteracts these drags, providing effectively infinite-time confinement at a chosen density. For the $\nu_{\perp\parallel}$ collision rate measurements, the rotating wall is turned off ~200 ms before the measurements, and turned back on after the measurement.

The plasma temperature is controlled by an ~4 mm wide cooling laser beam parallel to the magnetic field, illuminating essentially all the ions during one $\mathbf{E} \times \mathbf{B}$ drift rotation. This cooling beam is chopped at 250 Hz. When the cooling beam is blocked, the plasma temperature is diagnosed with a separate probe laser beam, which is frequency scanned across the transition. Both the cooling and the diagnostic beams excite the cyclic ${}^2S_{1/2}^{m_j=-1/2} \rightarrow {}^2P_{3/2}^{m_j=-3/2}$ (280 nm) transition, but the probe beam intensity is kept low enough to avoid distortion of the Maxwellian particle distribution.

Both $T_\parallel$ and $T_\perp$ are measured with the probe beam, by changing the beam orientation; however, the $T_\perp$ measurement has a substantial rotational broadening for $T < 10^{-4}$ eV, so we use only $T_\parallel$ to characterize the plasma temperature T. The equilibrium plasma temperature profile is broadly uniform near center, but often peaks 2× higher at the plasma edge. Moreover, cooling laser frequency variations cause temperature fluctuations up to 50% at the lowest temperatures.

We use two different techniques to measure the perp-to-parallel collision rate $\nu_{\perp\parallel}$. The first technique directly observes $T_\perp$ and $T_\parallel$ as they relax to a common value. The parallel temperature is initially increased by a small oscillating potential applied at one end of the plasma. This causes a variation ΔL in plasma length, with a consequent variation $\Delta T_\parallel / T \propto (\Delta L/L)^2$, resulting in $T_\parallel > T_\perp$.

Figure 7 shows the temporal evolution of $T_\parallel$ and $T_\perp$ during this technique, on a plasma with $n \sim 2 \times 10^7$ cm^{-3}. Before $t = 2$ s, an oscillating potential is applied to the end electrode and a steady state is reached, with $T_\parallel = 0.75$ eV and $T_\perp = 0.66$ eV. Here, the heating provided by the oscillating wiggle is balanced by cooling due to the residual background gas. At $t = 2$ s, the oscillating wiggle is turned off, $T_\parallel$ and $T_\perp$ relax to a common temperature at a rate $\nu_{\perp 0}$, while cooling due to the neutral background gas. We observe $(d/dt)(T_\parallel - T_\perp) = -\nu_{\perp 0}(T_\parallel - T_\perp)$ where $\nu_{\perp 0} = 3\nu_{\perp\parallel} + \nu_{iN}$, with ν_{iN} negligible for our measurements with $\nu_{\perp\parallel} > 1/\mathrm{s}$. An exponential fit to $T_\parallel - T_\perp$ gives $\nu_{\perp 0} = 6.8$ s^{-1}, to be plotted in Fig. 10 as $\nu_{\perp\parallel} = 2.3/\mathrm{s}$ at $T = 0.72$ eV.

This direct measurement technique is not practical when $\nu_{\perp\parallel} > 100$ s^{-1}; and it is not accurate for $T < 10^{-4}$ eV, since ion-neutral collisions give a heating rate $dT/dt \sim 0.6$

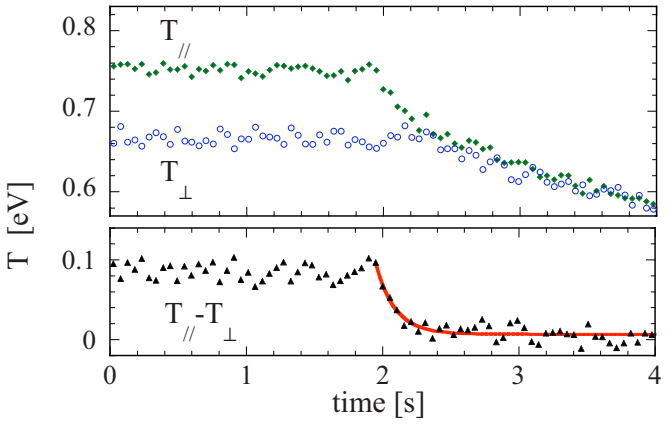

FIG. 7. (Color online) Directly measured relaxation of temperature anisotropy; the solid curve is the exponential fit to $T_{\parallel}-T_{\perp}$.

$\times 10^{-4}$ eV/s, which dominates the temperature evolution. We use the direct measurement technique essentially to confirm the results from the following "heating versus frequency" technique in the range of $T > 10^{-2}$ eV.

The heating versus frequency technique obtains the collision rate $\nu_{\perp\parallel}$ by determining the frequency $f_{\rm osc}$ at which axial compressions give maximal heating.[15] Here the initial plasma temperature is made as spatially uniform as possible, with a cooling laser balancing the background plasma heating due to neutral collisions, trap asymmetries, and electronic noise. A short oscillating burst ($3 \rightarrow 100$ cycles) at frequency $f_{\rm osc}$ is applied to a cylindrical electrode at one end of the plasma. As illustrated schematically in Fig. 8, the resulting heating is maximal when $2\pi f_{\rm osc} \sim \nu_{\perp\parallel}$. A three-dimensional adiabatic cycle occurs when $f_{\rm osc}$ is small, since $T_{\parallel}$ variations from ΔL can fully equilibrate with $T_{\perp}$. Similarly, when $f_{\rm osc}$ is large, little equipartition occurs, and a one-dimensional cycle ensues with no net heating.

More quantitatively, the heating due to the burst is maximal when $\nu_{\perp\parallel}=c(\Gamma)2\pi f_{\rm osc}$. Here, the specific heat has perpendicular and parallel components, giving $c(\Gamma)=c_{\parallel}c_{\perp}/(c_{\parallel}+c_{\perp})$, with $c_{\perp}=1$ and $c_{\parallel}=1/2+\partial U_{\rm corr}/\partial T$; the correlation energy $U_{\rm corr}$ is defined by Eq. (4.24) in Ref. 21. The specific heat increases slowly with correlation, with $c(0)=1/3$, $c(2) \simeq 0.42$, and $c(10) \simeq 0.52$.

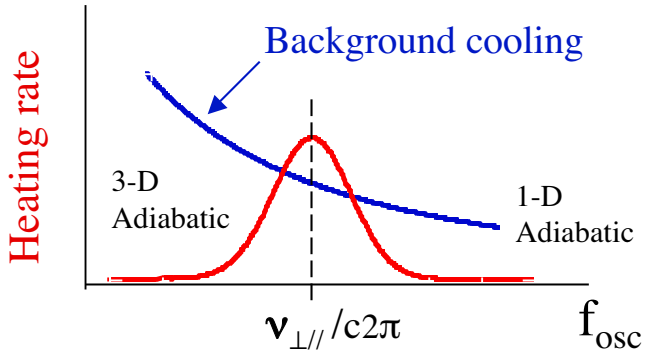

FIG. 8. (Color online) Conceptual sketch showing maximal heating when $f_{\rm osc} \sim 2\pi\nu_{\perp\parallel}$, exceeding background cooling only in a narrow range.

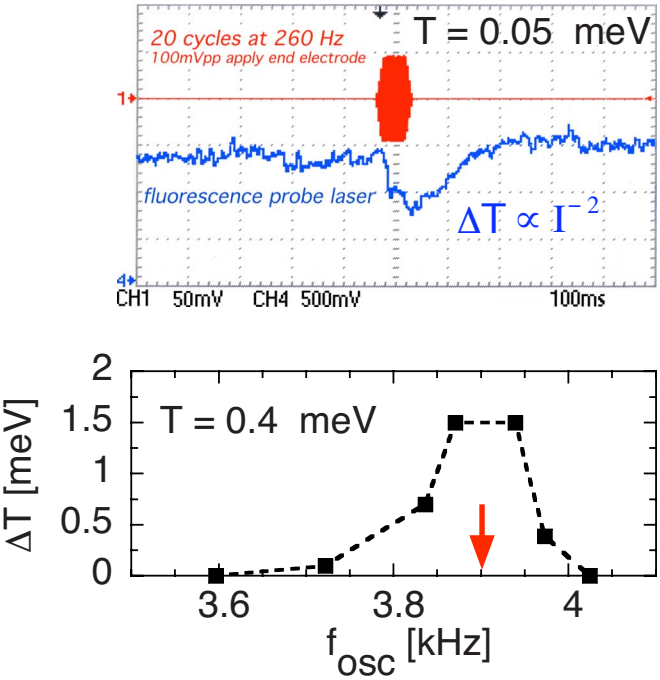

FIG. 9. (Color online) (a) Probe laser fluorescence showing ΔT caused by an optimal $f_{\rm osc}$. (b) Temperature increase vs frequency.

We measure the heating effect of the oscillating burst with a weak probe laser tuned to the resonant transition; the probe beam spans $0.2 \lesssim r \lesssim 0.3$ cm, and the fluorescence is recorded every 8 ms. Figure 9(a) shows the effect of a 20 cycle burst at 260 Hz on the probe laser signal for a plasma at temperature $T=3\times 10^{-5}$ eV: within a few cycles, the fluorescence drops by 30%; after the burst it slowly recovers due to the cooling laser. We adjust the oscillation amplitude so that the resulting heating is larger than background neutral cooling only at the optimal frequency, giving narrow, easily identified heating peaks. Figure 9(b) shows a typical heating peak, with a width of about 0.1 kHz at $f_{\rm osc}=3.9$ kHz, here for $T \sim 0.4$ meV.

These collisional heating maxima are distinct from heating due to resonant plasma modes. Plasma modes will also be excited by the oscillating burst, if $f_{\rm osc}$ is near a mode resonance. This gives a similar fluorescence signal, since a mode is an efficient way of coupling energy into the plasma and heating the particles. Fortunately, we are able to distinguish modes from collision maxima, since modes have only mild temperature dependence, and modes can be tracked over a wide temperature range. Also the persistent mode oscillations after the oscillating burst has stopped can be detected with other electrodes.

Figure 10 shows our measured $\nu_{\perp\parallel}$ versus temperature T for three different plasmas, compared to theory with and without correlation enhancements. The solid curves represent collisional theory without correlation effects, i.e., $I(\bar{\kappa})$ as calculated by Glinsky and plotted in Fig. 2; the dotted and dashed curves include the $f(\Gamma) \sim e^{\Gamma}$ correlation enhancement of Eq. (16). The higher density plasmas ($n=1.8$ and 2.0×10^7 cm^{-3}) become correlated at low temperature, with $\Gamma > 1$ for $T < 6\times 10^{-5}$ (dashed Γ). The lower density plasmas

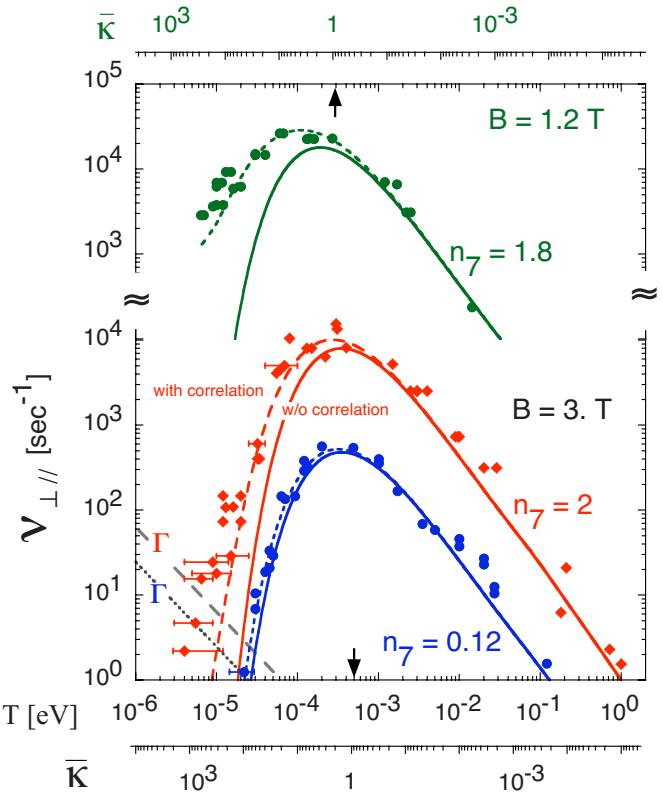

FIG. 10. (Color online) Measured collision rates for two densities and two B-fields vs temperature, compared to theory with and without correlations. The correlation parameter $\Gamma(T)$ for high and low density is also shown.

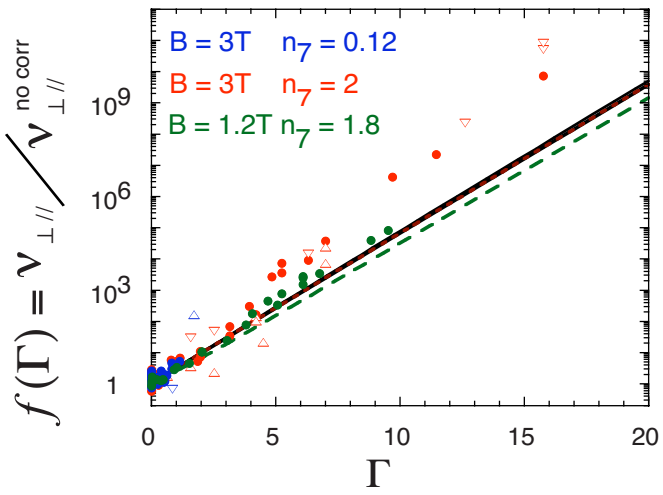

FIG. 11. (Color online) Measured enhancements $g(\Gamma)$ are consistent with "equilibrium shielding" estimates of Ichimaru (Ref. 5) (solid line) and Ogata (Ref. 9) (red dotted line) and DeWitt (Ref. 6) (green dashed line).

($n=0.12\times10^7$ cm^{-3}) barely reach $\Gamma=1$ at $T=2\times10^{-5}$ (dotted Γ), making the correlation enhancement barely noticeable.

Both sets of high density data are consistent with the "equilibrium shielding" correlation enhancement theory. The main experimental uncertainty at low temperatures arises from radially nonuniform and temporally varying plasma temperature. The coldest plasmas are systematically up to $2\times$ hotter at large radii, and the abscissa T represent density-weighted average temperatures. The eight error bars represent minimum and maximum $T(r)$ obtained from radial profiles. Plasma temperatures in the 10^{-5} eV range exhibit fluctuations because of temporal variation in the cooling laser frequency, and the error bars include this effect. The strong exponential dependencies in $I(\bar{\kappa})$ and $f(\Gamma)$ suggest that the observed equipartition would be dominated by the warmest regions of the plasma, i.e., the high T end of the error bars. The collisional heating during $f_{\rm osc}$ is inherently spatially averaged, and may also include undiagnosed spatial heat transport effects.

Figure 11 shows the measured $\nu_{\perp\|}$ collision rates of Fig. 10 divided by the theory prediction neglecting correlations [Eq. (1) and $f(\Gamma)=1$], giving the Salpeter enhancement $f(\Gamma)$. The experimental uncertainty in T translates into uncertainty in Γ, and into larger uncertainty in $f(\Gamma)$, through $I(\bar{\kappa})$. For clarity, only the lower and upper temperature ends of the eight error bars in Fig. 4 are plotted, as down-triangles and up-triangles, respectively. The solid line on Fig. 11 is Eq. (15) with no adjustable parameters. The estimate of Ogata[9] (red dotted line) is indistinguishable and that of DeWitt and Slattery[6] is well within the experimental uncertainty. The enhancement varies exponentially with correlation, in agreement with Eq. (15) up to $\Gamma\sim10$.

IV. DISCUSSION

It might seem odd that one can use thermal equilibrium screening potentials to determine the screening for particles with relative velocities far out on the tail of the Maxwellian velocity distribution. Most probably, *both* colliding particles have $v_\| \gg \bar{v}$ to obtain the large relative collision energy $E_\|$. Moreover, it is well-known that rapidly moving particles have strongly distorted Debye clouds. Recently, several papers[22] have been published that consider the effect such dynamical screening has on nuclear reaction rates; and some of these predict large deviations from the thermal equilibrium screening theory discussed here.

One can understand why using thermal equilibrium screening is in fact correct, even for high-velocity particles, through the following argument. The standard theory of screened reactions assumes that *all* phase-space configurations of the system are governed by the thermal equilibrium Gibbs distribution; this includes those rare configurations involving close collisions. If one then averages the reaction (equipartition or nuclear) over all phase space configurations that involve such close collisions, the velocity dependences in the Gibbs distribution factor out. One is then left only with a dependence on the configuration space of the particles surrounding the colliding pair; in other words, one obtains thermal equilibrium screening.

The data at two different B-field support the conclusion that the correlation enhancement f depends only on the thermal equilibrium parameter Γ, and is independent of the magnetization dynamics represented by $\bar{\kappa}$. Reducing B from 3 to 1.2 T decreases $\bar{\kappa}$ by $2.5\times$ at any T and provides a dramatic increase in $\nu_{\perp\|}(T)$ of Fig. 10 through $I(\bar{\kappa})$; but both data sets

are consistent with the same $f(\Gamma)$ enhancement. The experiments thus fully corroborate the Salpeter enhancement of collisionality in near-equilibrium correlated plasmas.

ACKNOWLEDGMENTS

This work was supported by National Science Foundation Grant No. PHY-0903877 and DOE Grant No. DE-SC0002451. We thank M. Affolter and C. Lee for assistance during some experimental runs.

[1] E. Schatzman, J. Phys. Radium **9**, 46 (1948).
[2] E. E. Salpeter, Aust. J. Phys. **7**, 373 (1954); E. E. Salpeter and H. Van Horn, Astrophys. J. **155**, 183 (1969).
[3] A. G. Cameron, Astrophys. J. **130**, 916 (1959).
[4] A. Alastuey and B. Jancovici, Astrophys. J. **226**, 1034 (1978).
[5] S. Ichimaru, Rev. Mod. Phys. **65**, 255 (1993).
[6] H. Dewitt and W. Slattery, Contrib. Plasma Phys. **39**, 97 (1999); A. Chugunov, H. E. DeWitt, and D. G. Yakovlev, Phys. Rev. D **76**, 025028 (2007).
[7] S. Ichimaru and H. Kitamura, Phys. Plasmas **6**, 2649 (1999).
[8] B. Jancovici, J. Stat. Phys. **17**, 357 (1977).
[9] S. Ogata, Astrophys. J. **481**, 883 (1997); S. Ogata, H. Iyetomi, and S. Ichimaru, *ibid.* **372**, 259 (1991).
[10] L. R. Gasques, A. V. Afanasjev, E. F. Aguilera, M. Beard, L. C. Chamon, P. Ring, M. Wiescher, and D. G. Yakovlev, Phys. Rev. C **72**, 025806 (2005).
[11] D. H. E. Dubin, Phys. Rev. Lett. **94**, 025002 (2005); Phys. Plasmas **15**, 055705 (2008).
[12] F. Anderegg, D. H. E. Dubin, T. M. O'Neil, and C. F. Driscoll, Phys. Rev. Lett. **102**, 185001 (2009).
[13] T. M. O'Neil and P. G. Hjorth, Phys. Fluids **28**, 3241 (1985).
[14] M. E. Glinsky, T. M. O'Neil, M. N. Rosenbluth, K. Tsuruta, and S. Ichimaru, Phys. Fluids B **4**, 1156 (1992).
[15] B. R. Beck, J. Fajans, and J. H. Malmberg, Phys. Rev. Lett. **68**, 317 (1992).
[16] M. J. Jensen, T. Hasegawa, J. J. Bollinger, and D. H. E. Dubin, Phys. Rev. Lett. **94**, 025001 (2005).
[17] A. W. Hyatt, C. F. Driscoll, and J. H. Malmberg, Phys. Rev. Lett. **59**, 2975 (1987).
[18] M. Jensen, T. Hasegawa, and J. J. Bollinger, Phys. Rev. A **70**, 033401 (2004).
[19] X.-P. Huang, F. Anderegg, E. M. Hollmann, C. F. Driscoll, and T. M. O'Neil, Phys. Rev. Lett. **78**, 875 (1997); F. Anderegg, E. M. Hollmann, and C. F. Driscoll, *ibid.* **81**, 4875 (1998); E. M. Hollmann, F. Anderegg, and C. F. Driscoll, Phys. Plasmas **7**, 2776 (2000).
[20] J. R. Danielson, C. M. Surko, and T. M. O'Neil, Phys. Rev. Lett. **99**, 135005 (2007).
[21] D. H. E. Dubin and T. M. O'Neil, Rev. Mod. Phys. **71**, 87 (1999).
[22] J. N. Bahcall, J. S. Brown, A. Gruzinov, and R. F. Sawyer, Astron. Astrophys. **383**, 291 (2002); N. Shaviv and G. Shaviv, Astrophys. J. **558**, 925 (2001).